Nebraska Public Power District

GENERAL OFFICE
P.O. BOX 499, COLUMBUS, NEBRASKA 68601-0499
TELEPHONE (402) 564-8561

LQA8300151

June 2, 1983

Director of Nuclear Reactor Regulation
Attention: Mr. Domenic B. Vassallo, Chief
Operating Reactors Branch No. 2
Division of Licensing
U.S. Nuclear Regulatory Commission
Washington, D.C. 20555

Subject: Mark I Containment Long Term Program - Plant Unique Analysis Report Loads Evaluation.
NRC request for information.

Dear Mr. Vassallo:

Attached for your review are our answers to the nineteen questions about our PUAR posed to us in April.

If you have any questions about our responses, please feel free to contact us.

Sincerely,

Jay M. Pilant
Division Manager of Licensing &
Quality Assurance

JMP:ck

Attachment

A025
1/1

ITEM 1

In the reference report NEDE-24840, it was shown that the absolute summation combination method for responses due to the CO load harmonics is overly conservative when compared to measured responses in FSTF tests. This is due in part to the random phasing of the 50 harmonics in the CO load, which is neglected in the absolute summation method. The study performed in the subject report used Monte Carlo random trials with LDR harmonics to generate cumulative distribution functions. NEDE-24840 concluded that a 50% NEP (3ASUM+47SRSS) was sufficient to envelop the FSTF test results. For CNS, an 84% NEP (4ASUM+46SRSS) was used for added conservatism.

For the CNS torus analysis, the displacement at 4 points at midbay were used to determine which 4 load harmonics gave the highest torus response. The maximum torus displacements were due to load harmonics in the following 4 frequency ranges: 5-6 Hz, 23-24 Hz, 24-25 Hz, and 26-27 Hz. The load frequency for each harmonic band was set to the midpoint of the frequency band, except when a torus natural frequency lay within the band. In this case, the torus natural frequency was assigned to the pressure component. Thus, the harmonic frequencies which produce the 4 highest torus responses were taken to be 5.5 Hz, 23.65 Hz, 24.22 Hz, and 26.5 Hz. For all torus response quantities, the responses due to the load harmonics at 5.5, 23.65, 24.22, and 26.5 Hz were added using absolute summation. The responses to the remaining 46 harmonics were combined by SRSS and added to the 4ASUM responses. The CNS analysis results and the NEDE-24840 report show similar reductions in response when the 4ASUM+46SRSS random phasing method is used.

The response combination method used at CNS was developed solely to consider the random phasing between the 50 load harmonics. Other conservative assumptions were made in the development and implementation of the CO load harmonics for CNS. These include:

- Three sets of alternate amplitudes for the baseline rigid wall pressure from 4 to 16 Hz were given in the LDR. The one set that maximizes response was to be used. For the CNS analysis, an envelope of the three sets was used for the 4 to 16 Hz range.
- The frequencies of the load harmonics were tuned to the torus natural frequencies, which maximized the torus response to each of the tuned harmonics. FSTF test results show no such tuning effect.
- The CO base harmonics generated by the LDR methods are generally conservative when compared to the loads measured in the FSTF tests, as discussed in NEDE-24840.
- Response of the FSTF facility with rigid end caps is conservative when compared to response of a continuous torus structure. Studies have indicated approximately a 30% decrease in wetwell response in actual plant configurations due to the phasing of pressure contributions from a number of downcomers.

The random phasing technique used at CNS is judged to be a reasonable and more realistic approach for combining torus response due to the 50 load harmonics. The loads used for the torus analysis have qualitatively been shown to be conservative; however, the final torus stress calculated for CNS gives quantitative indication of the degree of conservatism. The maximum torus stresses due to CO loads at CNS were 8.4 ksi (membrane) and 10.4 ksi (surface). This is significantly higher than the maximum stress of 2.9 ksi measured in all FSTF tests (including M12); therefore, the design methods used for the CNS analysis are considered to contain adequate conservatism.

ITEM 2

The methodology used to develop the 1.2 SRSS technique for torus shell pressures due to multiple S/RV actuations is discussed in detail in Appendix A of the PUAR. Pressure wave characteristics for the worst-case valve actuations were determined for the S/RV discharge lines at CNS using computer programs RVFOR04 and QBUBS02. From those plant-unique analyses, relationships for peak pressure amplitudes, frequency of the pressure wave, water clearing time, and time decay multiplier as a function of valve opening time were generated.

Valve opening time, valve set point variation, and reactor pressure rise rate all affect the pressure wave characteristics in the torus. Each variable is random within certain ranges of occurrence. The distribution frequency of each variable was obtained from generic BWR 4 (reactor pressure rise rate and valve set point variation) and Mark I (valve opening time) studies. Four hundred Monte Carlo trials were performed using the plant-unique relationships and randomly generated parameters.

Five cases of multiple actuation were studied in the analysis program. Using a 1.2 multipler on the SRSS combination of peak shell pressures, ranges of NEP at the 95% confidence level were calculated for the five cases. These ranges are reported in Table 2.1. Note that a 95% confidence level was actually used in the studies, although a 90% confidence level was stated in the PUAR.

As can be seen in Table 2.1, the 1.2 SRSS method provides an extremely high NEP for the first four cases, with a minimum NEP of 98%. For the 8MVA case, the lower bound NEP is 84%, and the upper bound NEP is 91%.

The SRSS methodology was first used in 1976 for the combination of loads due to multiple valve actuations for Mark III plants. Because there was no precedent, an arbitrary criterion of 95% NEP with 95% confidence level was proposed by GE.

In 1978, a similar SRSS methodology was developed by GE for use on Mark II plants. GE Report NEDO-21061, Rev. 3, July 1978, suggested a 90% NEP with 90% confidence level for multiple valve actuations during an IBA, SBA, or NOC, and an 85% NEP with 85% confidence level for multiple valve actuations during a DBA. Multiple valve actuation tests performed at Caorso showed the conservatism of the Mark II load definition; thus the 90% NEP with 90% confidence level was accepted by the NRC for use on Mark II plants.

It should be noted that the lower bound NEP of 84% is for the 8MVA case only. The probability of occurrence of the 8MVA event is extremely low. For the CNS analysis, the bounding multiple valve actuation case was 6ADS. For this case, a lower bound NEP of 99% was observed. Thus, the 1.2 SRSS method is considered conservative with respect to the final design loads.

Monticello in-plant S/RV tests have also indicated the conservatism of the Mark I LDR loads for multiple valve actuations. The maximum torus pressure reported in the Monticello tests was 7.0 psi. A single valve actuation case bounded the results of all tests, with pressures due to multiple valve actuations of similar magnitude. The maximum torus pressure calculated for CNS was 20.5 psi. This pressure is significantly higher than the Monticello test pressure; therefore, the 84% NEP used at CNS is judged to be adequate and reasonable for the torus design.

TABLE 2.1

Non-Exceedence Probabilities of 1.2 SRSS Method
for Multiple S/RV Actuation Torus Shell Pressures (95% Confidence Level)

S/RV Multiple Actuation Case	Non-Exceedence Probability (%)	
	Lower Bound	Upper Bound
3ADS	99	100
6ADS	99	100
3MVA	99	100
6MVA	98	100
8MVA	84	91

ITEM 3

During an IBA/SBA event, the drywell is pressurized by the blowdown from the break. The air/steam mixture in the drywell is then purged into the wetwell through the vent system and into the S/RV discharge lines through the vacuum breakers located inside the drywell. These vacuum breakers have a low set point of 0.2 psid and will remain open until the pressures in the S/RV discharge lines are close to the drywell pressure. Consequently, the S/RV discharge lines will contain an air/steam mixture and not pure air. Further, the controlling load case for the torus analysis is the 6ADS event at maximum torus internal pressure. Maximum wetwell pressure is determined assuming that most of the drywell air has been purged into the wetwell, leaving the remaining drywell atmosphere mostly steam.

In NUREG-0661, Section 3.10.2.6, it is stated that "the S/RV line will contain a mixture of air and steam at a high pressure...but with a lower air volume." With this statement in mind, it was assumed that equal volumes of air and steam exist in the S/RV discharge lines. For this air/steam mixture at drywell conditions of 260°F and 35 psia, a relative humidity of approximately 50% is obtained. In the CNS analysis, the relative humidity was further reduced to 30%.

ITEM 4

The Technical Specifications for CNS require that the PAS be isolated within 15 seconds of receipt of the Group 2 isolation signal. Actual closure time for the four isolation valves ranges between 6.4 and 8.2 seconds. This closure time is checked quarterly per Surveillance Procedures.

ITEM 5

Presently, 16 resistance thermometers (RTDs) measure temperature downstream of the 8 T-quenchers, as discussed in Section 1.3.4.4 of the PUAR. Although the RTDs measure temperature locally, they are not placed in locations where maximum local temperatures will be measured. However, these RTDs are placed such that the temperatures measured by the sensors provide reasonable estimates of the suppression pool bulk temperature.

In Section 7 of the PUAR, it was shown that, if the bulk pool temperature prior to a LOCA is held below the 95°F limit provided in the Technical Specifications, the local pool temperature limit of 200°F will not be exceeded in the event of a LOCA. Therefore, the present pool temperature monitoring system is designed to prevent the temperature at each RTD from exceeding the 95°F normal operating limit. Plant operators may introduce cooling water to the torus and/or start the RHR system to lower the bulk temperature or to equalize the temperature distribution between torus bays.

The future plant process computer will not be installed at CNS for 1-2 years. Present plans for suppression pool temperature monitoring, using the computer, are to continue to insure that the 95°F temperature limit at any RTD is not exceeded during normal operations. No plans have been made to perform more detailed bulk or local pool temperature calculations with the computer.

ITEM 6

Revision 2 of the PULD was issued to update the pressure and temperature transients for the increase in initial temperature of the CNS suppression pool to 95°F during the summer months. The initial pool temperature was 90°F in Revision 1. The changes in the transients are discussed below:

- DBA temperature and pressure transients were provided for zero ΔP in Revision 2. They were not reported in Revision 1. The only differences between the Revision 1 transients used in containment design and the Revision 2 transients at zero ΔP are in the maximum wetwell temperature and pressure. Here the difference is less than 1%, which is a negligible difference.

- The IBA and SBA maximum wetwell temperatures increased. The IBA maximum wetwell temperature increased from 157°F to 162°F. The SBA maximum wetwell temperature increased from 123°F to 134.4°F. The CNS torus was analyzed for temperature response as described in Section 3.2.3.2.1. A maximum temperature of 200°F was used; thus the temperature increases in Revision 2 of the PULD have no impact on the CNS analyses. The pressure transients for the IBA and SBA events did not change from Rev. 1 to Rev. 2.

ITEM 7

The effective pool mass resisting the upward displacement was derived using the methodology in Appendix D of NEDE-21944-P. The value of 0.74 (fraction of water in flight) reported for CNS (zero ΔP) was based on the downcomer submergence of 4.375 ft. used in the original QSTF tests. The downcomer submergence at CNS was decreased to 3.333 ft., which caused a decrease in the loads seen by the torus. For a submergence of 3.333 ft., the percentage of water in flight was calculated to be 59% of the total mass at zero ΔP, using the same methodology as in NEDE-29144-P.

ITEM 8

Figure 2.13 in the CNS PUAR shows the corrected torus net vertical loads. Longitudinal and azimuthal multipliers were obtained from LDR Table 4.3.2-1 and were matched to the times corresponding to the events in the load transients in Figure 2.13. For $z/l = 0.0$ and $\theta = 180°$, the following multipliers result for given times:

Time		$M_z(z/l = 0.0)$	$M_\theta(\theta = 180°)$
Start of Accident	0 msec	1.0	1.0
Peak Download	230 msec	0.852	1.205
Zero Download	405 msec	1.059	0.947
Peak Upload	490 msec	1.109	0.908
Reduced Upload	670 msec	1.077	0.963
Zero Upload	1320 msec	1.0	1.0

Figure 2.14 in the CNS PUAR shows the corrected average submerged pressure used with the multipliers shown above to obtain pressure transients at selected locations. The given multipliers were used to obtain multipliers at specific points on the torus by linear interpolation. Multipliers at specific times between the peaks were also obtained by linear interpolation. A computer program was developed to perform these interpolations. The design pressure transients for specific points were obtained by the equation in the LDR:

$$P_{loc.sub}(t) = P_{avg.sub}(t) \times M_z \times M_\theta$$

An example curve for $z/l = 0.0$ and $\theta = 180°$ is attached as Figure 8.1.

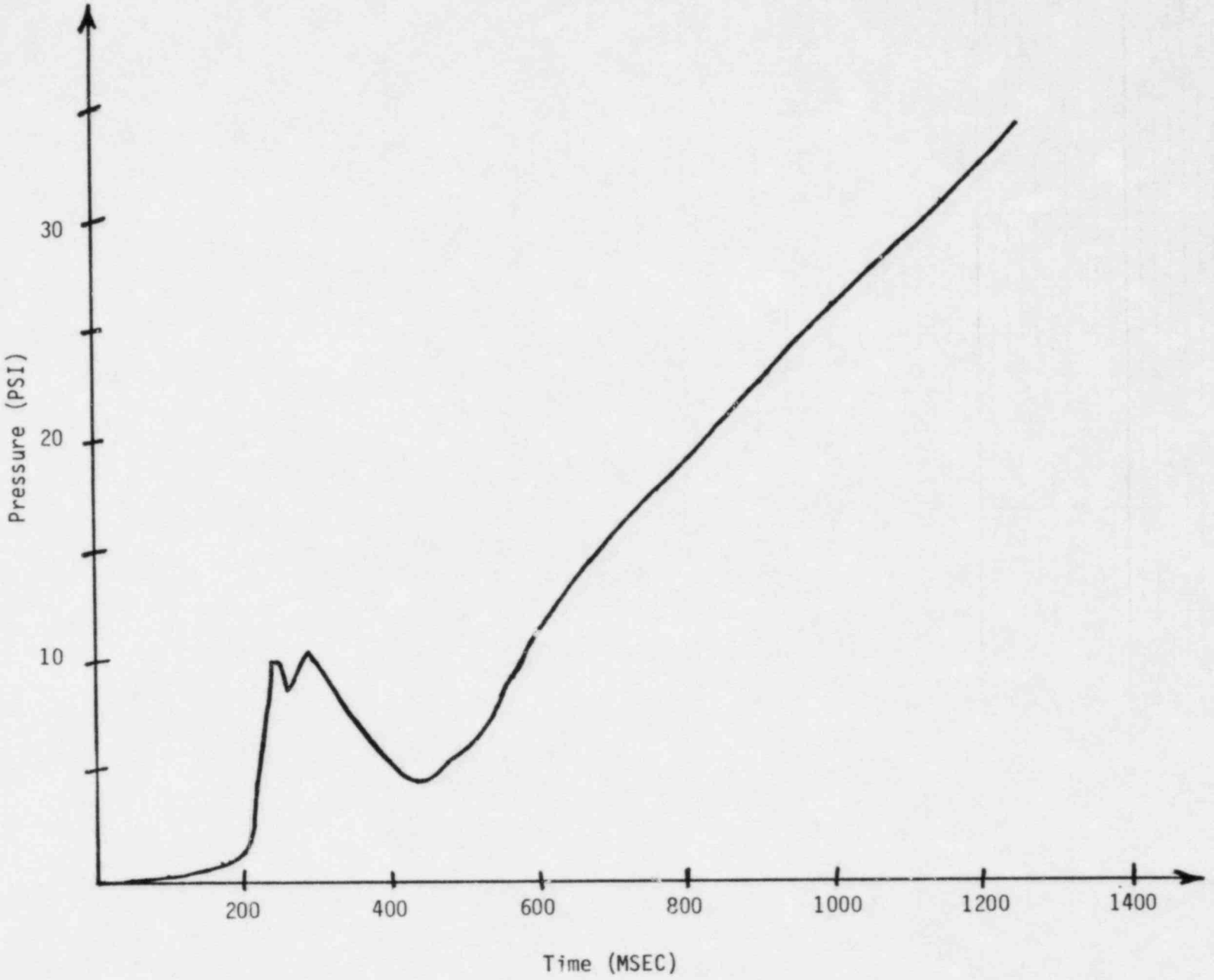

FIGURE 8.1
Torus Submerged Pressure Transient at z/l = 0.0 and θ = 180°

ITEM 9

To perform the finite element analysis of the vent header system, it was necessary to obtain a complete set of load profiles for the entire impacted area of the vent header. It was assumed that the entire lower surface of the vent header ($\theta = 0°$ through $\theta = 60°$) was subjected to impact and drag loads. Since load profiles were not provided for each angular location (0°, 15°, 30°, 45°, 60°) at the longitudinal locations, interpolation and extrapolation schemes were utilized to obtain those profiles.

For the location in question ($\theta = 60°$, z/l = 0.92), the basic load profiles corresponding to Location B (T_2, T_4, T_6, T_9) shown in Figure 2.16 of the PUAR were used to develop the transient for the specific location. The basic load profile for $\theta = 60°$ at Location B was first obtained by using quadratic extrapolation of the time and pressure values from transients T6 ($\theta = 30°$) and T9 ($\theta = 45°$). This basic load profile was used in all longitudinal locations B. The longitudinal variation relationships were then used to determine the required load profile for the specific location.

ITEM 10

In the suppression pool, the velocity of the fluid flowing between submerged structures is significantly lower than the acceleration of that fluid. The drag forces on the submerged structures due to that acceleration are obtained by calculating an equivalent added mass on the structure of interest. The interference effects are then determined as a ratio of drag forces determined with and without the interfering structure.

A computer program was developed to evaluate the interference effects. The submerged structures are modeled as cylinders with finite elements on the boundary surface. In the analysis model, the fluid remains stationary, and the cylinders move with the negative fluid velocity. An iterative solution is used to define the complete velocity potential around the cylinder by distributing singularities along the surface.

The acceleration drag forces are then evaluated using the double integral over the cylinder surface:

$$F_D = \rho \frac{dU}{dt} \iint_S \phi_1 U_{n1} dS$$

where

ρ = fluid density

$\frac{dU}{dt}$ = fluid acceleration

ϕ_1 = normalized velocity potential

U_{n1} = normalized velocity normal to cylinder surface

The interference effect for a particular cylinder is calculated by first determining the ratio of the acceleration drag force with the interfering cylinder in the flow field to the acceleration drag force with no interfering cylinder. The multiplier to be used with the Mark I loads is then obtained:

$$\text{Multiplier} = (1 + \frac{F_{DI}}{F_D})/2$$

where

F_{DI} = acceleration drag force with interfering cylinder in model

F_D = acceleration drag force with no interfering cylinder in model

The computer program was verified by comparison to published data (References 1, 2) on fluid flow between submerged structures.

The computer program was used to perform a sensitivity study to investigate the effect of the variation of submerged structure configurations on the interference effects calculated for those structures. For structures not within 30° of being parallel, upper bound factors were developed for groups of structures with similar configuration. The total interference factor for a structure was

ITEM 10 (Cont'd.)

obtained by summing the interference effects due to all other structures as follows:

$$A_T = 1.0 + A_{I1} + A_{I2} + \ldots + A_{Ii} + \ldots + A_{In}$$

where
A_T = total interference factor
A_{Ii} = interference factor due to structure i
n = number of structures producing interference effects

The upper bound interference factors are given in Table 10.1. The interference effects multipliers given in Table 2.8 of the PUAR were derived using the factors in Table 10.1 and factors for structures within 30° of being parallel. The latter interference factors were derived using the methodology in the AC.

References:

(1) "Potential Flow Past a Group of Cylinders," C. Dalton and R. A. Halfinstine, Transactions of the ASME, Dec. 1971.

(2) "Wave Forces on Cylinders Near Plane Boundary," T. Yamamoto, J. H. Nath, and L. S. Slotta, Journal of the Waterways, Harbor, and Coastal Engineering Division, Nov. 1974.

TABLE 10.1
Upper Bound Interference Factors

Configuration	Upper Bound Interference Factor, A_I
Structures in the same plane, included angle is greater than 30°	1.0
Structures not in the same plane, greater than (D_O + D_I) apart	0.3
Structures not in the same plane, less than (D_O + D_I) apart	1.0
Structures less than 1.5D_I from the torus shell	0.3

Notes: D_I = equivalent cylinder diameter for structure of interest
D_O = equivalent cylinder diameter for interfering structure

ITEM 11

The baseline rigid wall load multiplication factor of 0.91 for CNS was based on the smallest pool-to-vent area ratio for the torus bays. A non-vent bay with six downcomers was the bounding case.

ITEM 12

Reference 26 of the PUAR has already been transmitted to the NRC. The criteria used to include FSI effects for submerged structures are as specified in the AC and are clarified below:

- Torus shell analyses were performed to obtain shell accelerations.
- The computer program CONDFOR was used to determine the local fluid accelerations at the submerged structures due to CO at the downcomers.
- The CONDFOR accelerations were then compared to the maximum calculated shell accelerations at each 1 Hz frequency band. If the maximum shell acceleration was greater than one-half the CONDFOR acceleration, then FSI effects were included in the load calculation for the frequency band.
- The methodology in Reference 26 of the PUAR was used to calculate the FSI effects. These effects were substantial, as can be seen in the load calculation for a section of the S/RV discharge piping, presented in Table 12.1.

The FSI effects for the submerged structures were unrealistic when calculated using the methodology of the AC. For the S/RV discharge piping, the FSI effects calculated were in excess of 15 times the CO source load. At certain load frequencies, the FSI effects were over 100 times the source load. Therefore, a reasonable upper bound limit to the total FSI effect on all submerged structures was necessary.

An energy balance study was performed to calculate the maximum response of the S/RV discharge piping possible given the finite input energy in the CO event. First, the maximum available energy was determined, using a conservative estimate of total mechanical energy input to the suppression pool through the downcomers from the start of the CO event to the time of maximum response of the torus and the 24" T-quencher support pipe. It was then assumed that only the torus and 24" pipe absorb energy, which maximizes the response of the piping by neglecting the response of the other submerged structures.

In order to assess the FSI effects on the S/RVDL, the lower bound torus kinetic energy was calculated and subtracted from the input energy to give an upper bound energy available to be imparted to the 24" support pipe:

$$E_{pipe} = E_{input} - E_{torus}$$

The 24" support pipe energy can be thought of as strain energy absorbed by the support pipe due to the CO source and FSI loading of the S/RV discharge piping. The displacement of the 24" support pipe due to the absorption of the available strain energy was calculated. This displacement was then attributed to the FSI load only. The displacement of the 24" support pipe due to CO load only was previously calculated; thus a ratio of FSI load to CO load could be determined.

The ratio of FSI load to CO source load for the 24" support pipe was approximately 10. It should be noted that this is an upper bound estimate because of the conservatism of the assumptions made to maximize the remaining energy due to FSI effects. This factor was used only in the evaluation of the responses of the S/RVDL and supports.

TABLE 12.1
Maximum T-Quencher Drag Loads
Due to Condensation Oscillation

Frequency, Hz	Source Load lbf/ft	FSI Effect lbf/ft	Ratio FSI/Source
5.5	28	15	0.5
15.5	1	27	27.0
21.5	3	304	101.0
23.5	3	289	96.0
26.5	6	220	37.0
35.5	1	15	15.0
45.5	3	54	18.0
4ASUM + 46SRSS of Frequency Bands	90	1,390	15.0

ITEM 13

The chugging acoustic downcomer pressure oscillation amplitude used for the CNS evaluation was $\pm$13.0 psi. This value was inadvertently omitted in the PUAR.

ITEM 14

In Section 2.13.7 of the AC, the requirements for consideration of the asymmetric S/RV discharge state that the load case which maximizes the asymmetric condition shall be considered. For CNS, the load condition used for analysis was the actuation of all 8 S/RVs with phasing adjusted such that the horizontal load in one direction would be a maximum.

For the analysis of the torus shell, the ring girders and saddles sufficiently isolate the response of each bay such that the out-of-phase actuation of S/RVs several bays away has an insignificant effect on the response due to S/RV actuation in the bay. The components which are affected by the asymmetric S/RV discharge are the seismic ties, which resist net lateral load on the torus structure. The loads due to the worst-case asymmetric discharge were used in the evaluation of the seismic ties. This worst case involves 4 T-quenchers on one half of the torus discharging such that the pressure load is maximized in the outboard direction in each quencher bay. The 4 T-quenchers on the other side of the torus discharge to maximize the pressure load in the inboard direction. In this way, the net horizontal load on the torus was maximized and used for the seismic tie design. Figure 14.1 illustrates the concept.

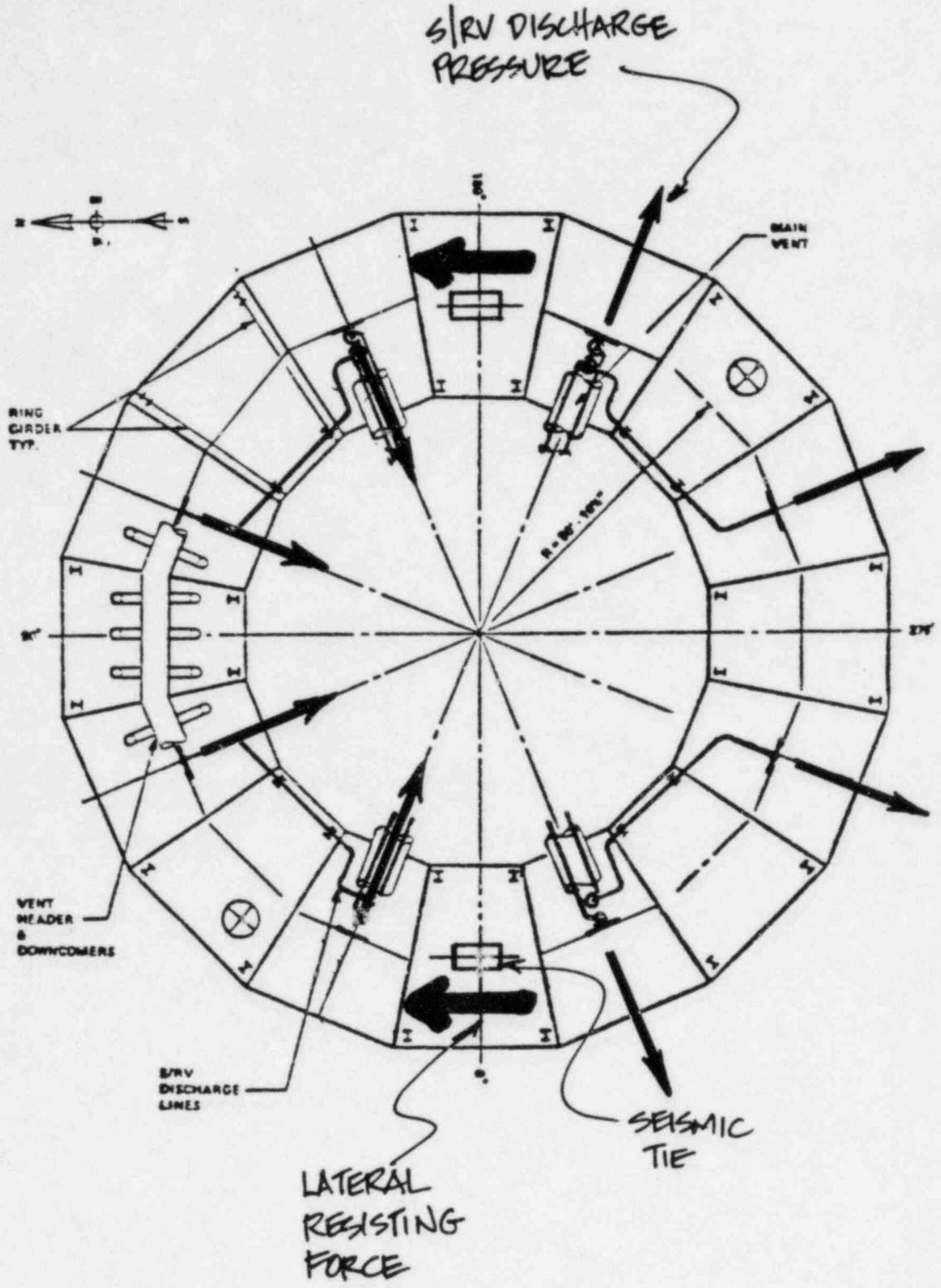

FIGURE 14.1

Asymmetric S/RV Discharge Loads

ITEM 15

The T-quencher used in the CNS plant is identical to the T-quencher tested at Monticello. Figure 1-2 of GE report NEDE-21935-P, "Mark I Containment Program - T-Quencher Load Definition Report," August 1978, shows the hole pattern for the generic Mark I T-quencher.

ITEM 16

The knockdown factor applied to the predicted column reactions was derived by comparing the results of the Monticello T-quencher tests to analytical results for the same loading condition using the computer program QBUBS03. Program QBUBS03 calculates the maximum pressure load seen by the torus at Bottom Dead Center (BDC) and includes the 1.65 bounding factor as specified in Section 2.13.3.2 of the AC. This pressure was attenuated in the longitudinal and circumferential directions, giving a uniform, bounding distribution of load along the torus surface, compared to a non-uniform distribution of load observed in the Monticello test. Vertical forces on the tributary areas for each column were then summed, and column loads were calculated and compared to the measured load at Monticello. For the test case giving the highest torus loads, the upper bound ratio between the test load and the calculated load was 0.6, and this was used as the knockdown factor for torus column loads calculated with the predicted pressure distribution.

ITEM 17

The listed computer programs were developed and maintained by General Electric. All programs were verified by GE, and QA documents were provided to NPPD for all programs installed on the CDC system. EDS used the computer programs without making any revisions, and proper use was assured through general checking procedures as required by the EDS QA program.

ITEM 18

The local pool model discussed on page 7-3 was presented to the NRC at a meeting on December 17, 1982. At the present time, the NRC and General Electric are discussing the applicability of the model for all Mark I plants. The model was used to determine the bulk to local temperature difference for CNS as intended by GE. As this issue is generic to the Mark I program, the response to this item is deferred until resolution of the issue is achieved.

ITEM 19

The models used for the development of post-chug loads on the ring girder are shown in Figures 19.1 and 19.2 attached. Vent #1 in Figure 19.1 was the primary vent used for the maximum source and phasing evaluation. Analyses were performed to investigate the effects of phasing between Vents #1 and #2 and Vents #1 and #9 to obtain maximum forces and moments on the ring girder.

The set of source strength vs. frequency values for the post-chug event was obtained from the methodology in Section 4.5.2.1 of the LDR. The peak source strength was 377.83 ft^3/sec^2 at a 26 Hz load frequency. The post-chug analysis was performed at the peak source strength and respective frequency. Pressure loads at all other frequencies are directly proportional to source strength, and loads at each frequency were obtained by scaling the results of the peak source strength analysis by the ratio of source strength at the frequency of interest to peak source strength. This ratio is the same as the ratio of torus wall pressure at the frequency of interest to the torus wall pressure at 26 Hz.

The ring girder, attached to the torus shell and stiffened by gussets, is essentially a rigid structure when compared to the frequencies of the load harmonics considered. Confirmatory structural analysis was performed to verify that the natural frequency of the ring girder is significantly higher than the 50 Hz cutoff frequency for the load harmonics. Therefore, no DLFs were applied to the loads.

The submerged portion of the ring girder was divided into ten segments as shown in Figure 19.2. The drag volume of a ring girder segment was calculated by considering the volume of an equivalent cylinder of diameter D_{eq} as specified in Section 2.14.2 of the AC. Figure 19.3 shows the calculation of the drag volume for the ring girder. The associated drag coefficient used was 2.3.

Loads on the ring girder due to chugging were calculated with the program CONDFOR, using the worst-case phasing between vents. For in-plane forces in the X and Y directions, the case of vents #1 and #9 in-phase was determined to give the highest forces on the ring girder. For out-of-plane force in the Z-direction, two cases were considered. First, Vents #1 and #9 were taken to be out-of-phase; then Vents #1 and #2 were taken to be in-phase. The former case was found to control. Table 19.1 presents the maximum forces for the peak source strength.

The accelerations at the ring girder segment centroids calculated by CONDFOR were then used to determine the FSI effects on the structure. The FSI calculations were performed using a computer program which used the CONDFOR accelerations, maximum torus shell accelerations, accelerations at the ring girder segment centroids due to torus shell accelerations, and interference effect multipliers to determine the final ring girder design loads. Figure 19.4 shows the flow chart of the program.

The CONDFOR accelerations used are reported in Table 19.2. These accelerations are for the peak source amplitude. The local accelerations for each frequency band were determined by scaling the results of the peak source case by appropriate factors. These were then compared to the maximum shell acccceleration determined for each frequency band in the torus shell analysis. FSI effects were included if twice the maximum shell acceleration exceeded the local

ITEM 19 (Cont'd.)

(CONDFOR) acceleration. The local effects of the torus acceleration were calculated using the method in Reference 26 of the PUAR, and these accelerations were used to calculate the FSI-induced loads. Interference effects were included as a scale factor applied to the loads. These factors are calculated in Table 19.3.

Final loads for ring girder evaluation were obtained by absolute summation of the peak loads for each of the 50 load harmonics. In-plane loading of the ring girder was considered in the 1/32 model torus analysis, but because symmetric boundary conditions were used at the ring girder plane, out-of-plane loads were considered separately. The absolute summation of peak loads in the Z-direction was applied quasi-statically to the ring girder, and the resulting stresses were added to the stresses calculated in the torus analysis. Table 19.4 shows the calculation of the load in the Z-direction on segment 5 of the ring girder. These net section forces were assumed to act uniformly over the segment surface. Pressure loads on the ring girder were developed from the forces and were used in the structural evaluation.

Table 19.1
Maximum Forces for Peak Source Strength

Ring Girder Section	Vents #1, #9 In-Phase		Vents #1, #9 Out-of-Phase
	F_x, lbf	F_y, lbf	F_z, lbf
1	64.6	-16.8	138.2
2	-396.1	241.7	383.2
3	-566.6	631.9	511.7
4	-240.5	512.7	451.2
5	-22.9	155.4	318.3
6	18.4	124.4	179.3
7	53.5	114.0	90.0
8	35.5	39.6	46.8
9	-19.1	-11.6	24.6
10	-40.0	-10.4	8.2

Table 19.2
Maximum Accelerations for Peak Source Strength

Ring Girder Section	Vents #1, #9 In-Phase		Vents #1, #9 Out-of-Phase
	A_x, ft/sec^2	A_y, ft/sec^2	A_z, ft/sec^2
1	-1.86	-9.44	1.19
2	-6.69	-3.28	3.30
3	-6.48	4.02	4.41
4	-0.909	4.97	3.89
5	3.55	1.89	2.74
6	4.45	0.440	1.55
7	3.20	-0.302	0.776
8	1.78	-0.983	0.403
9	0.721	-1.55	0.212
10	0.134	-1.93	0.0707

Table 19.3
Interference Effects Factors on Ring Girder

Submerged Structure	Interference Factor		
	Segments 1-4	Segments 5-6	Segments 7-10
Torus Shell	N/A	N/A	N/A
24" and 10" Support Pipes	0.30	1.00	0.30
End Plates	N/A	0.06	N/A
T-Quencher Arms	N/A	N/A	N/A
HPCI Exhaust Piping	N/A	N/A	0.42
RCIC Exhaust Piping		Bounded by HPCI	
Base Factor	1.00	1.00	1.00
TOTAL	1.30	2.06	1.72

NOTE: N/A = Not Applicable, no interference effects.

Table 19.4
Out-of-Plane Loads for Ring Girder Segment 5

Frequency, Hz	Chugging Load, lbf	FSI Load, lbf	Chugging + FSI Load, lbf
0.5	20.4	0.0	20.4
1.5	20.4	0.0	20.4
2.5	17.6	0.0	17.6
3.5	16.8	0.0	16.8
4.5	29.6	0.0	29.6
5.5	29.0	0.0	29.0
6.5	32.2	1.0	33.2
7.5	32.1	1.4	33.5
8.5	32.2	1.7	33.9
9.5	32.1	2.1	34.2
10.5	149.7	1.3	151.0
11.5	129.8	0.7	130.5
12.5	69.9	6.4	76.3
13.5	61.2	3.4	64.6
14.5	11.6	0.8	12.4
15.5	10.6	2.6	13.2
16.5	5.4	1.7	7.1
17.5	7.1	4.8	11.9
18.5	5.1	9.6	14.7
19.5	28.6	79.3	107.9
20.5	29.8	28.7	58.5
21.5	52.2	55.8	108.0
22.5	157.3	45.4	202.7
23.5	157.4	89.5	246.9
24.5	229.0	70.2	299.2
25.5	534.5	50.6	585.1
26.5	643.4	298.4	941.8
27.5	428.9	206.4	635.3
28.5	278.1	121.8	399.9
29.5	198.6	45.7	244.3
30.5	73.5	9.4	82.9
31.5	36.7	2.5	39.2

Table 19.4 (Cont'd.)

Frequency, Hz	Chugging Load, lbf	FSI Load, lbf	Chugging + FSI Load, lbf
32.5	64.5	2.5	67.0
33.5	86.1	5.1	91.2
34.5	72.4	7.9	80.3
35.5	105.4	18.2	123.6
36.5	71.4	27.5	98.9
37.5	35.7	22.1	57.8
38.5	41.6	35.2	76.8
39.5	50.0	3.1	53.1
40.5	382.9	97.0	479.9
41.5	383.0	67.0	450.0
42.5	383.0	18.2	401.2
43.5	383.0	4.1	387.1
44.5	383.0	4.0	387.0
45.5	383.0	3.5	386.5
46.5	383.0	3.0	386.0
47.5	382.9	3.1	386.0
48.5	383.0	3.5	386.0
49.5	383.0	7.5	390.5
TOTAL	7,917.7	1,473.7	9,391.4

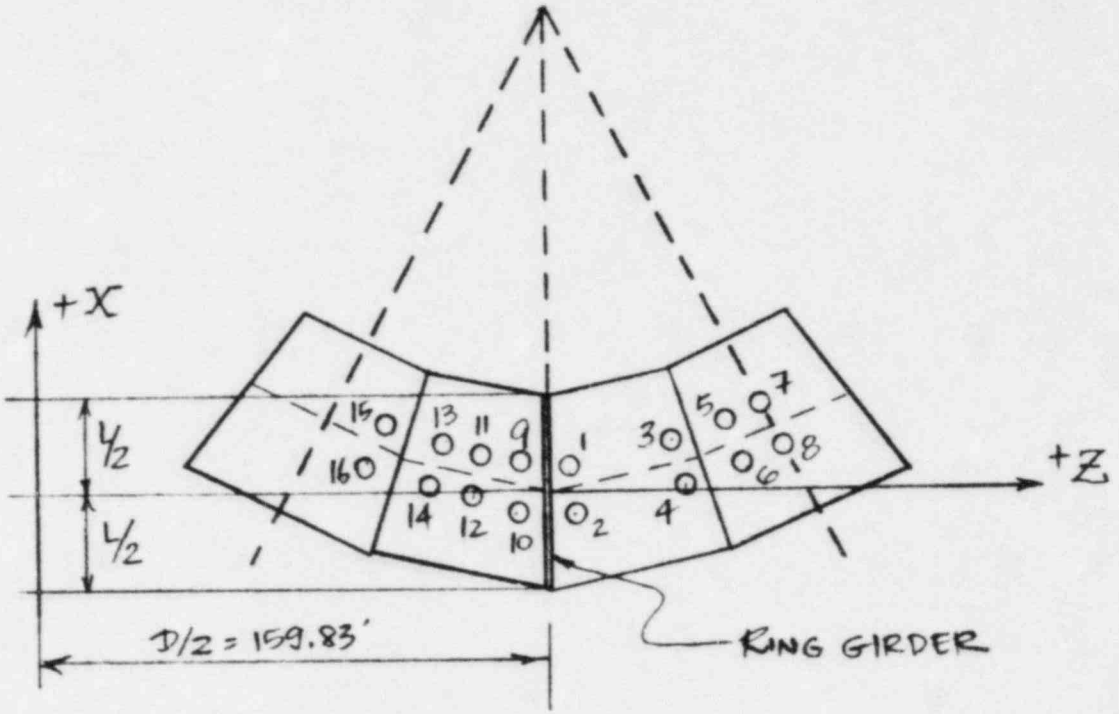

FIGURE 19.1

Suppression Pool Cell Geometry

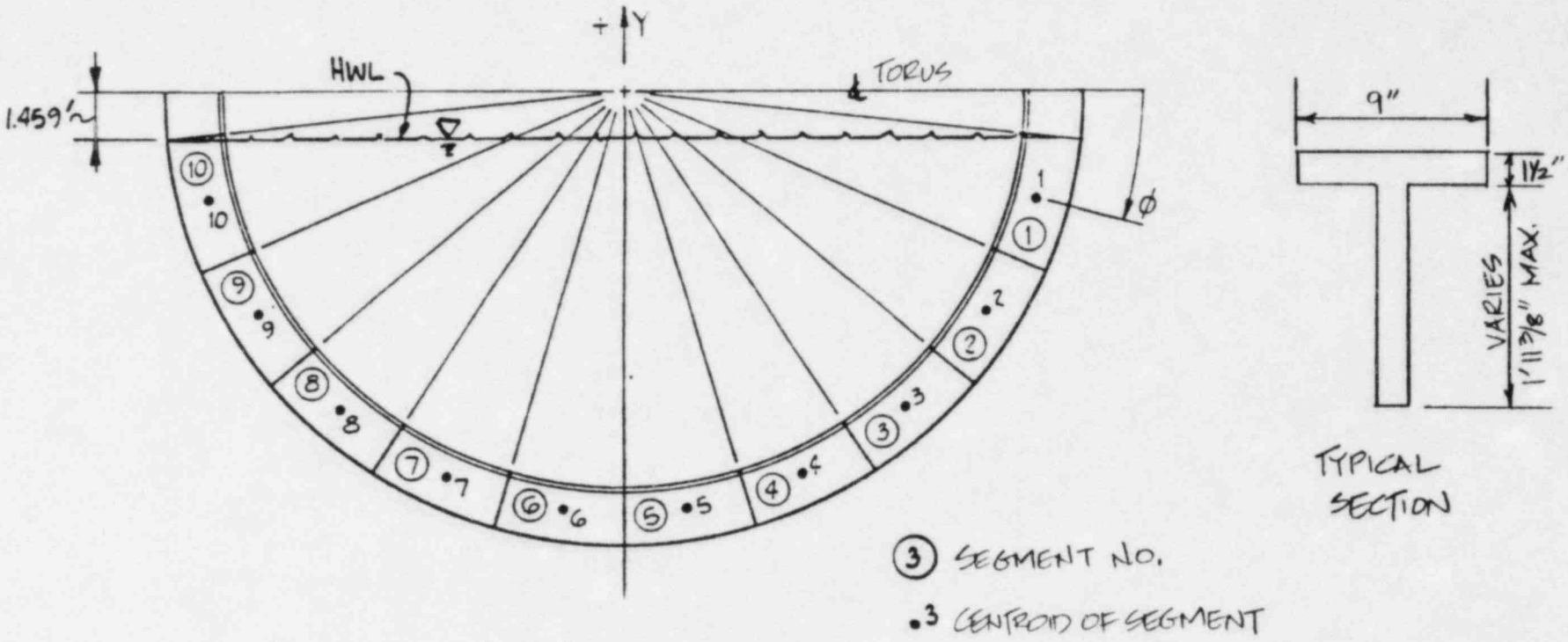

FIGURE 19.2
Ring Girder Geometry

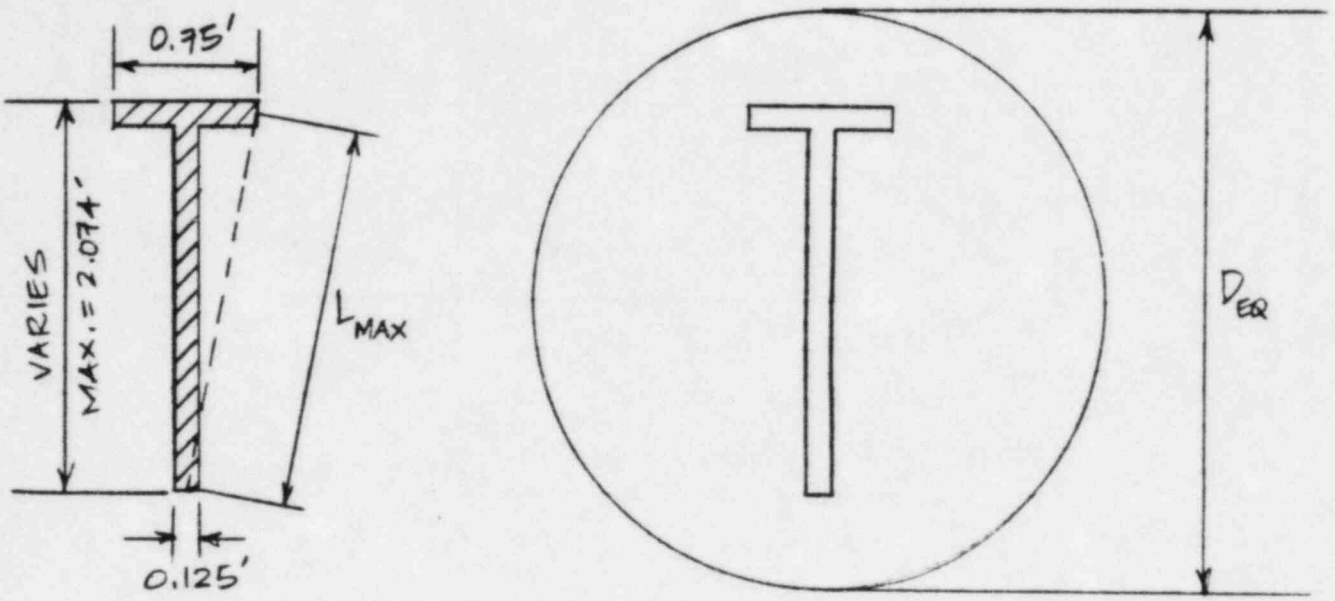

$$L_{max} = \left[\left(\frac{0.75 + 0.125}{2}\right)^2 + (2.074)^2\right]^{1/2} = 2.12 \text{ ft}$$

$$D_{eq} = \sqrt{2} L_{max} = 2.998 \simeq 3.0 \text{ ft}$$

L_s = Section length = 3.9 ft

V_d = Drag volume = $\frac{\pi}{4} (D_{eq})^2 (L_s)$

$= \frac{\pi}{4} (3.0)^2 (3.9) = 27.6 \text{ ft}^3$

C_D = Drag coefficient = 2.3

Figure 19.3
Ring Girder Drag Volume

For each frequency band:

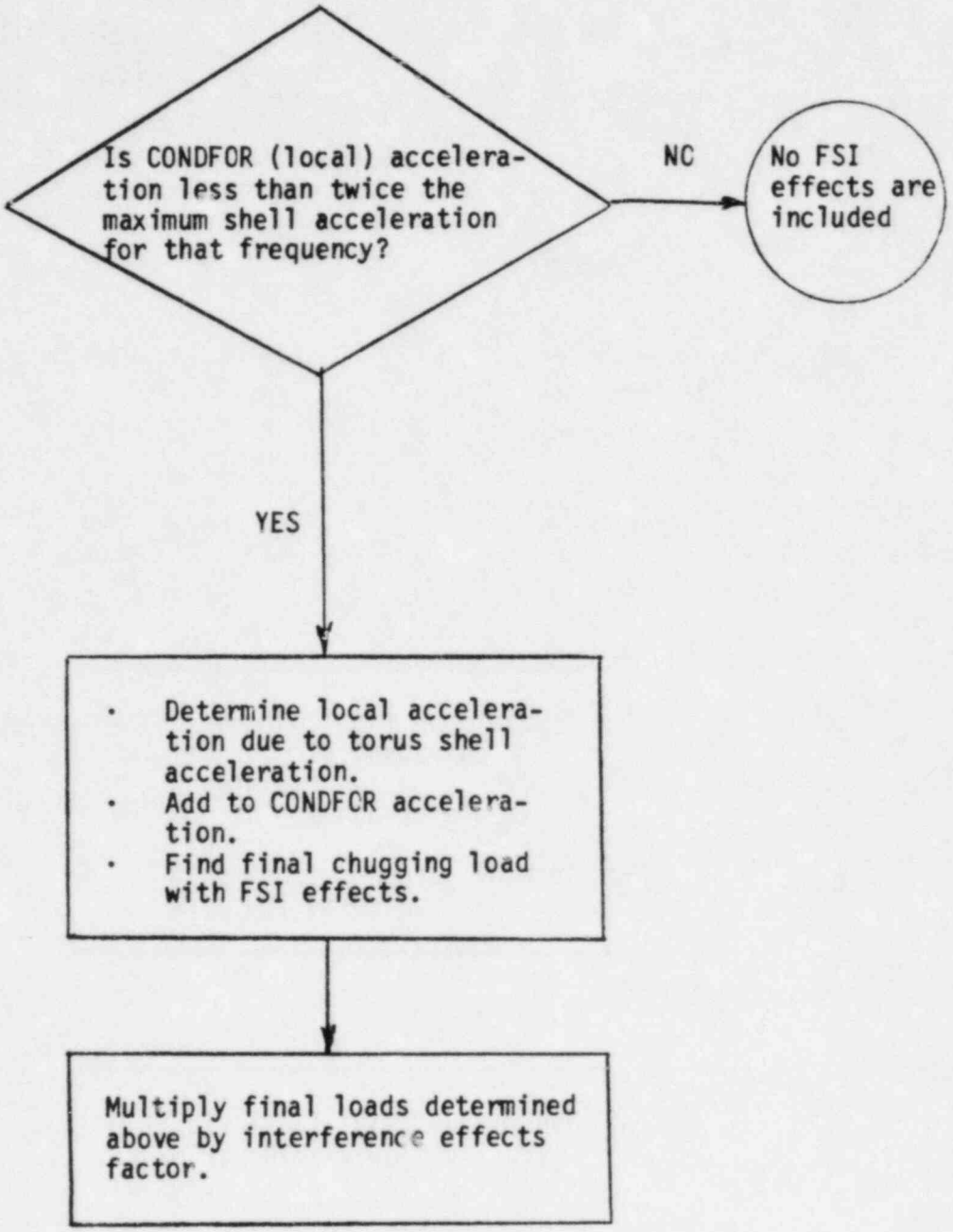

Figure 19.4
FSI Effects Flow Chart